Parasitic Capacitance E_{qoss} Loss Mechanism, Calculation, and Measurement in Hard-Switching for GaN HEMTs

Ruoyu Hou, *Member*, *IEEE*, Juncheng Lu, *Member, IEEE*, and Di Chen, *Member*, *IEEE*
GaN Systems Inc.
Ottawa, Canada
E-mail: rhou@gansystems.com

***Abstract*— Gallium Nitride enhancement-mode high electron mobility transistors (GaN E-HEMTs) can achieve relatively high-efficiency and high-frequency in hard-switching mode. One particular reason is that GaN E-HEMTs obtain zero reverse-recovery loss and also a zero reverse-recovery period. For silicon (Si) MOSFETs, it has been a well-known issue that their Q_{rr} is too big to switch the transistor in hard-switching mode. Researchers have made extensive efforts to calculate the reverse-recovery loss. However, few of them pay attention to the Q_{oss}, as the Q_{rr} dominates in the turn-on switching loss for Si MOSFETs. For GaN HEMTs, the absence of the Q_{rr} makes the Q_{oss} noticeable, although the value of the Q_{oss} for GaN HEMTs is still the smallest among both Si and Silicon Carbide (SiC) MOSFETs. This paper focus on the E_{qoss} loss in GaN HEMTs. The E_{qoss} loss mechanism, detailed calculation and detailed measurement method for GaN HEMTs are provided. In addition, the theoretical results are verified by the double-pulse test at different junction temperatures and gate resistances.**

***Index Terms*—GaN HEMT, gallium nitride, double pulse test, switching loss, parasitic capacitance loss, turn-on loss, E_{qoss} loss.**

I. Introduction

Compared with silicon (Si) MOSFETs, Gallium Nitride enhancement-mode high electron mobility transistors (GaN E-HEMTs) have gained high popularity recently due to their better figures of merit (FOM) and their great potential for enabling higher switching frequencies, higher efficiencies, and higher power densities for power converters [1-3]. Its applications include, but are not limited to, point of load converters, power adapters, LED drivers, automotive DC/DC converters, battery chargers, PV inverters, motor inverters and wireless power [4-11].

The hard-switching turn-on of Si MOSFET and GaN HEMT are shown in Fig. 1 and Fig. 2, respectively. Due to the existence of the body diode in the Si MOSFET, the reverse-recovery Q_{rr} makes the device hard to work in the hard-switching mode, especially under relatively high switching frequency. For GaN HEMTs, due to the absence of the body diode, the current I_d waveform is relatively clean. This enables the GaN-based power electronic systems can do hard-switching at relatively high switching frequency. Nevertheless, a small current bump generated by Q_{oss} can still be observed and thus

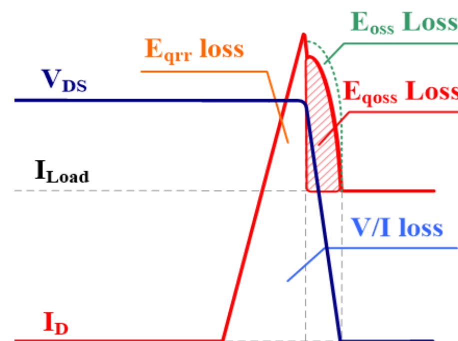

Fig. 1: Hard-switching turn-on loss of Si MOSFET.

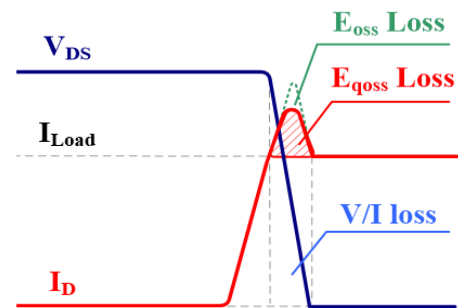

Fig. 2: Hard-switching turn-on loss of GaN HEMT.

the energy loss E_{qoss} is introduced. Although the value of the Q_{oss} in GaN HEMTs is still the smallest among both Si and Silicon Carbide (SiC) MOSFETs, the absence of the Q_{rr} in GaN makes this current bump noticeable. This energy loss E_{qoss} is not E_{oss}, which is also known as the capacitance self-charging/discharging energy. Moreover, the loss E_{qoss} cannot be calculated in the same way as E_{qrr} loss because during that period, the switch voltage V_{ds} is no longer a constant value and it already starts falling. In [12-14], the authors mentioned this energy loss is due to the discharge of the capacitance at the switching node. However, the detailed analysis, measurement method and measurement results have not been presented. The calculation of the E_{qoss} is important, as 1) it can provide a more accurate calculation for the turn-on switching loss energy E_{on};

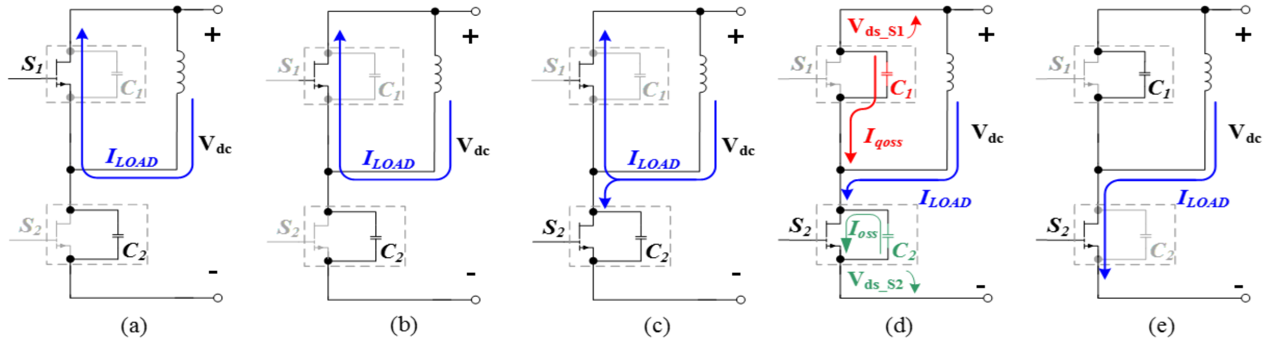

Fig. 3: Hard-switching transition, (a) S_1 conducting, (b) Deadtime, (c) Current commutation, (d) Voltage commutation, (e) S_2 conducting.

2) it also enables the users to scale the E_{on} to other V_{ds} voltage precisely [15].

The rest of the paper is organized as follows: Section II presents the E_{qoss} loss mechanism and calculation. The analysis of the effect of other parasitic capacitances on the E_{qoss} loss is discussed in Section III. The E_{qoss} loss measurement method and its experimental verification are presented in Section V. Finally, conclusions are given in the Section VI.

II. E_{QOSS} Loss Mechanism and Calculation

A. E_{qoss} loss mechanism

A typical hard-switching transition for GaN E-HEMTs is shown in Fig. 3. S_1 is the synchronous switch and S_2 is the active switch. Once the switch S_1 is turned off, deadtime loss occurs. As soon as S_2 is turned on, the current commutation starts. Due to the absence of body diode of GaN HEMT, once the current in S_2 reaches the load current I_{LOAD}, the voltage commutation will start right away. During the voltage commutation period, the voltage across S_1 increases and the voltage across S_2 decreases. Accordingly, the capacitor C_1 and C_2 will be charged and discharged, respectively. As the two-dimensional electron gas (2DEG) of S_2 is already conducting, the C_2's self-discharging current will flow into S_2's 2DEG, which generates the E_{oss} loss. However, E_{oss} loss cannot be measured directly as the current flows internally from C_2 to S_2's 2DEG. In the meanwhile, the 2DEG of S_1 is already turned off. Therefore, according to the KCL, the C_1's charging current will also flow through S_2 and generate a current bump, which yields the E_{qoss} loss.

Therefore, it can be summarized that the E_{oss} loss is introduced by the capacitance self-discharging current of the switch device itself and E_{qoss} loss is introduced by the capacitance charging current from the opposite switch device. As discussed in [15], the switching loss distribution in GaN HEMTs is shown in Table I.

TABLE I. Summary of Switching Loss Distribution in GaN HEMTs

Loss distribution	Theoretical	Measured
Turn-on loss E_{on}	$E_{VIon} + E_{qoss} + E_{oss}$	$E_{VIon} + E_{qoss}$
Turn-off loss E_{off}	E_{VIoff}	$E_{VIoff} + E_{oss}$

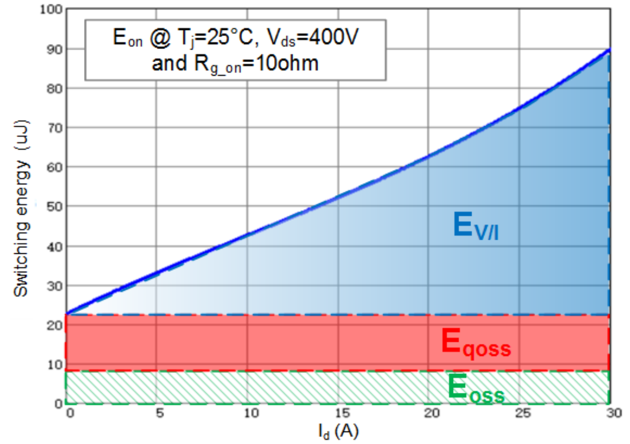

Fig. 4. E_{on} loss distribution for GS66508T.

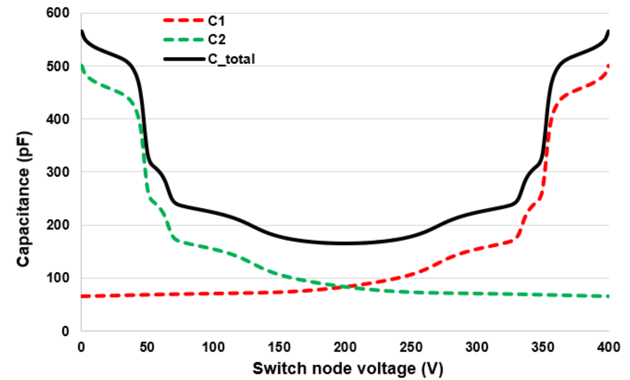

Fig. 5. Switch node capacitance of GS66508T.

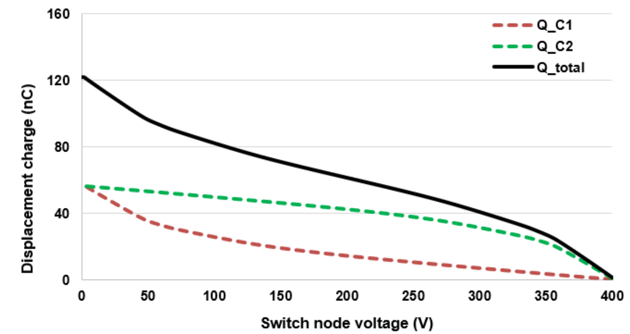

Fig. 6. Displacement charge of GS66508T with V_{dc}=400V.

Fig 4 shows the E_{on} loss distribution for GS66508T at T_j=25°C, V_{ds}=400V and R_{g_on}=10Ω. Clearly, E_{qoss} and E_{oss} loss affect the overall E_{on} loss, especially under light load operating condition where the channel current I_d is relatively small. Therefore, accurate E_{qoss} and E_{oss} loss calculations are necessary in order to obtain an accurate overall E_{on} loss.

B. E_{qoss} loss calculation

As the parasitic capacitance C_{oss} is dependent on the voltage V_{ds}, a switch node capacitance example can be plotted in Fig. 5, if GS66508T is applied. Accordingly, the displacement charge can also be plotted in Fig. 6. Clearly, with the switch node voltage decreased from 400V to 0V, the total amount of charge for each C_1 and C_2 during the voltage commutation period are exactly the same. However, the loss of E_{oss} and E_{qoss} are not the same. The equations to calculate the E_{oss} and E_{qoss} can be derived as below,

$$E_{oss} = \int_0^{V_{dc}} V_{ds} \cdot C_{oss(V_{ds})} dV_{ds} \tag{1}$$

$$E_{qoss} = \int_0^{V_{dc}} (V_{dc} - V_{ds}) \cdot C_{oss(V_{ds})} dV_{ds} \tag{2}$$

From the above two equations, the E_{oss} and E_{qoss} losses under different operating voltages for GS66508T can be obtained in Fig. 7. It is clear that the E_{qoss} loss is higher than E_{oss} loss. The reason is that usually the capacitance C_{oss} of the device is higher at lower voltage V_{ds} region. In fact, for Si MOSFET, most likely, as its capacitor C_{oss} is more nonlinear than GaN, its E_{qoss} loss will be even larger. An E_{qoss} loss comparison between Si MOSFET and GaN HEMT under different operating voltages is shown in Fig. 8.

III. Analysis of Other Parasitic Capacitances on the E_{QOSS} Loss

It needs to be point out that during the circuit-level testing, the measured parasitic capacitive energy loss E_{oss}/E_{qoss} not only includes the parasitic capacitance of the semiconductor device, but also the parasitic capacitances from PCB and inductor. If double-pulse test (DPT) circuit is applied, the parasitic capacitances distribution can be plotted in Fig. 9. The parasitic capacitances C_{pcb} and C_{pl} are not voltage-dependent, but they also contribute to the E_{oss} and E_{qoss} loss. Therefore, by taking the capacitances C_{pl} and C_{pcb} into account, the complete equations to calculate the E_{oss} and E_{qoss} for this circuit are,

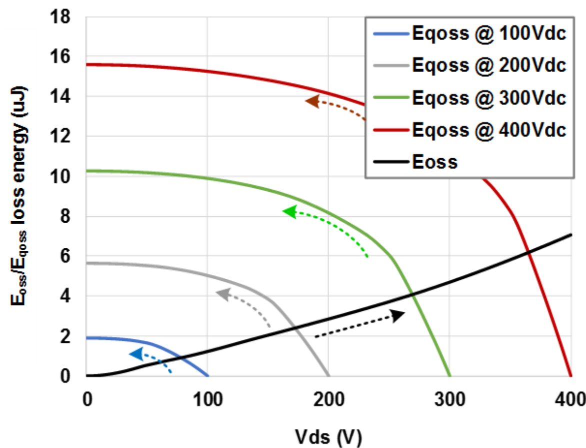

Fig. 7. E_{oss}/E_{qoss} loss of GS66508T at different operating voltage.

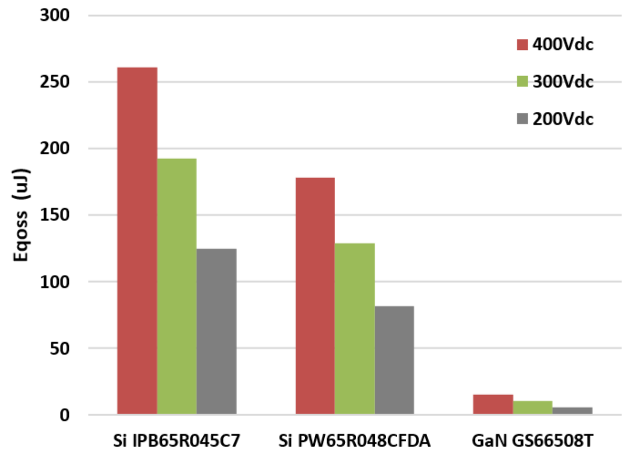

Fig. 8. E_{qoss} loss comparison between Si MOSFET and GaN HEMT.

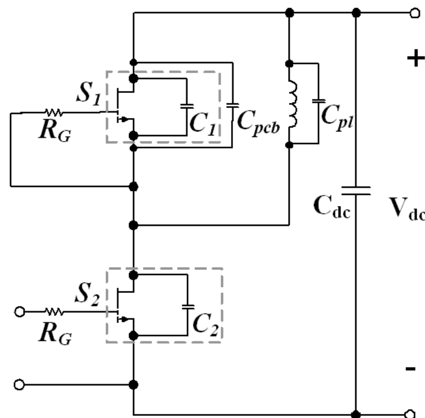

Fig. 9. Parasitic capacitances distribution of E_{qoss} loss in DPT circuit.

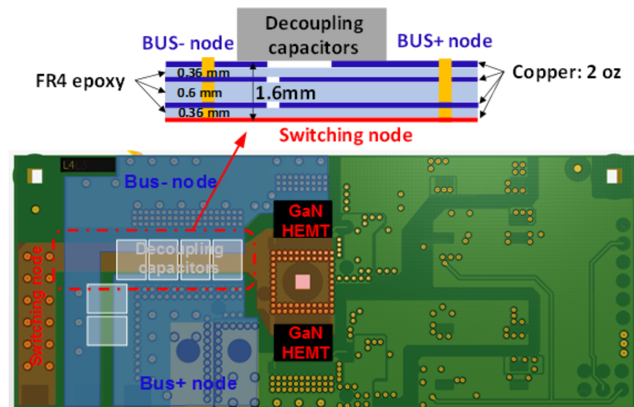

Fig. 10. PCB parasitic capacitance from switching node to bus+/- node.

$$E_{oss} = \int_0^{V_{dc}} V_{ds} \cdot C_{oss(V_{ds})} dV_{ds} + \frac{1}{2}(C_{pl} + C_{pcb})V_{dc}^2 \quad (3)$$

$$E_{qoss} = \int_0^{V_{dc}} (V_{dc} - V_{ds}) \cdot C_{oss(V_{ds})} dV_{ds} + \frac{1}{2}(C_{pl} + C_{pcb})V_{dc}^2 \quad (4)$$

In order to extract the parasitic capacitance value from the PCB of the testing setup, a Q3D simulation has been performed for the GS66508T evaluation board [16]. The PCB parasitic capacitance from switching node to bus node is shown in Fig. 10. The simulated PCB parasitic capacitance is 14 pF. By adding other parasitic capacitances together, the total voltage-independent capacitance is about 20 pF in this case.

IV. E_{QOSS} Loss Measurement Method and Experimental Verification

The E_{qoss} loss should be only relevant to the capacitor charging energy. In other words, the loss should only be a function of voltage V_{ds} and the parasitic capacitance which is mainly the C_{oss}. Therefore, most likely, load current I_{Load}, junction temperature T_j and switching speed should not affect the E_{qoss} loss value. In this section, the load current independence is verified first. Then, a simple E_{qoss} loss measurement method is presented and a DPT with closed-loop temperature control is built up. The junction temperature and switching speed independence are both verified by this test setup.

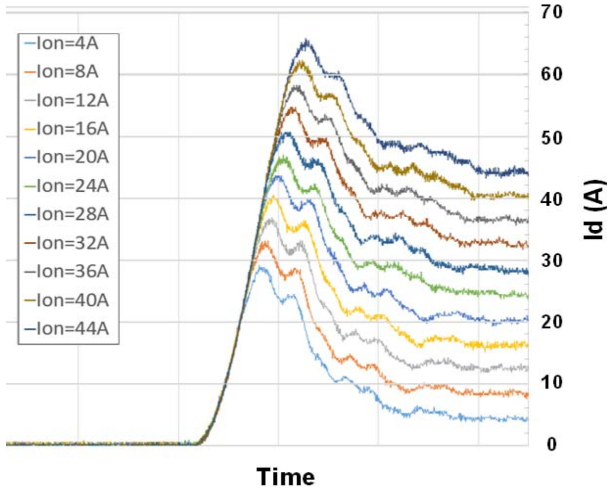

Fig. 11. Measured I_d current waveforms of GS66516T under different load currents.

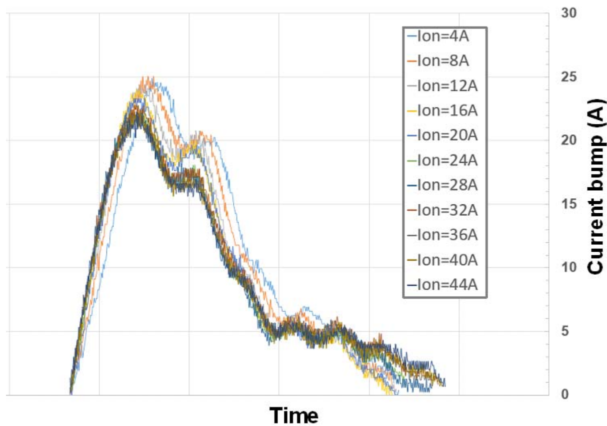

Fig. 12. Current bump comparison of GS66516T under different load currents.

A. *Load current independence*

It is important to verify the load current independence for the E_{qoss} loss of GaN, as this can also verify the absence of body diode in GaN HEMT. It is well known that for Si MOSFET, the Q_{rr} loss is dependent not only on the load current, but also on the *di/dt* rate [17-18]. This makes the hard-switching E_{on} loss calculation relatively difficult and complicated for Si MOSFET. Unlike to Si MOSFET, the zero Q_{rr} loss of GaN HEMT not only results in a lower E_{on} loss, but also leads to a more accurate and more straightforward E_{on} loss calculation than Si MOSFET.

Several double pulse testings based on GS66516T under different load currents were performed. The I_d current waveforms are shown in Fig. 11. To better observe the current bump generated by the Q_{oss}, the current bump comparison under different load current are zoomed and shown in Fig. 12. It is clear that the current shapes are about the same, which indicates the load current independence.

B. *E_{qoss} loss measurement method*

In order to verify the impact factor and also the value of the loss, the DPT platform with closed-loop temperature control is applied. The device under test (DUT) is GS66508T and the setup is shown in Fig. 13 [15]. The junction temperature of the device is monitored by an NTC thermistor. A power resistor is applied to heat up the device accordingly.

During the DPT, the E_{qoss} can be measured either upon turn-on of the first pulse or on the turn-on of the second pulse as shown in Fig. 14. However, the E_{on} on the second pulse includes both E_{qoss} loss and the IV overlapping loss. Since the load current is zero at the turn-on of the first pulse, all the loss should be contributed by E_{qoss} only, which simplifies the loss measurement. Therefore, in this paper, the E_{qoss} is measured at the turn-on of the first pulse.

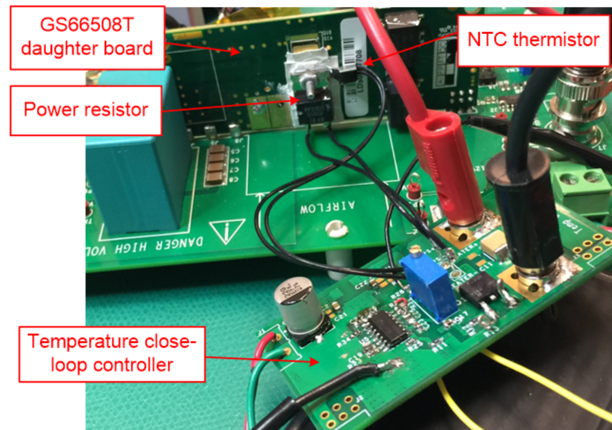

Fig. 13. DPT setup with junction temperature control [15].

C. Junction temperature and switching speed independence

Fig. 15 shows the measured first pulse waveforms under different operating voltage V_{dc}, T_j, and external R_{g_on}. As the purpose of the test is to prove the switching speed independence and also measure the E_{qoss} energy loss as accurate as possible, in this paper, the R_{g_on} is chosen as 30 ohm and 50 ohm, respectively. Therefore, relatively clean waveforms can be obtained in Fig. 15.

Fig. 16 summarizes all the test results. It indicates that the E_{qoss} is also independent on the junction temperature and switching speed. Fig. 17 shows the comparison between the measured and calculated results. It is clear that by considering the other parasitic capacitances from the PCB and power inductor, the discrepancy between the theoretical values and measured values is relatively small, verifying the calculation method.

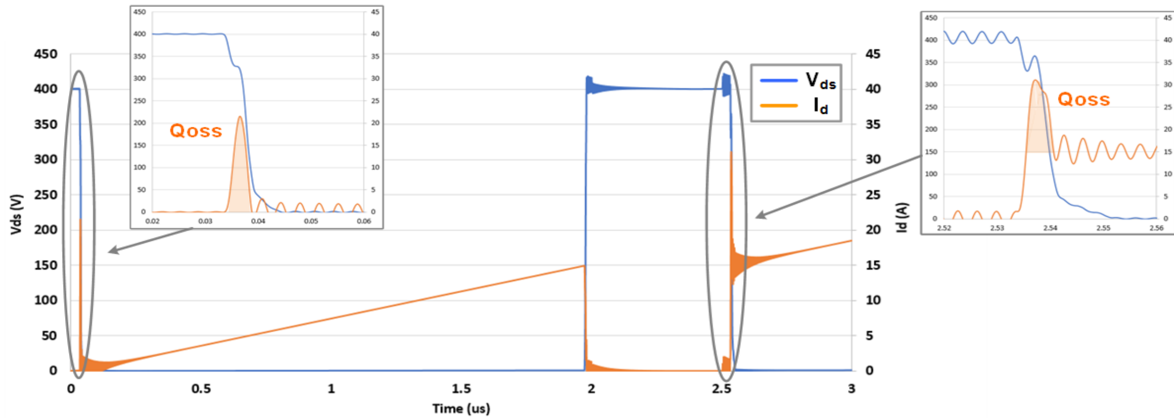

Fig. 14. Two possible E_{qoss} Measurement methods in DPT.

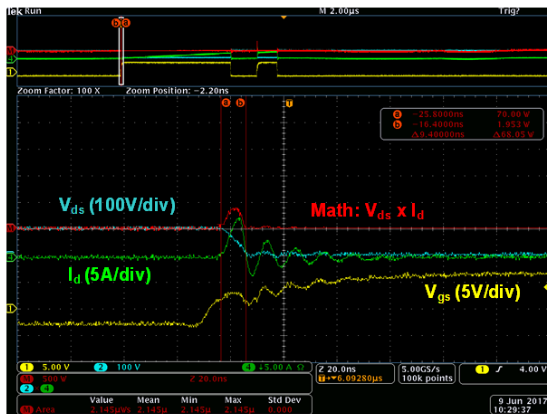

(a)

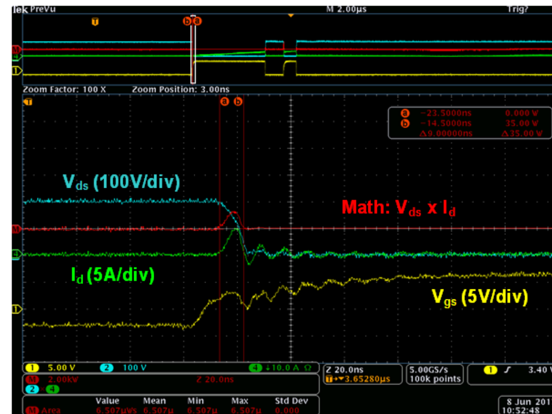

(b)

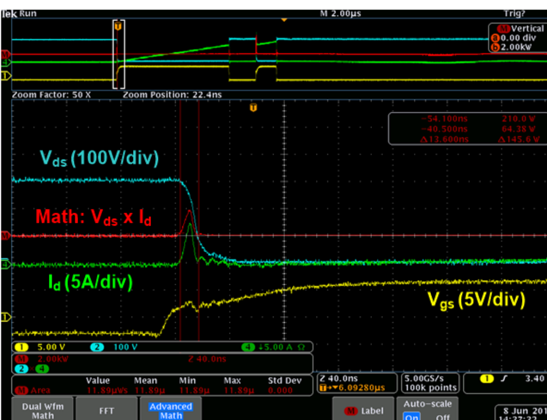

(c)

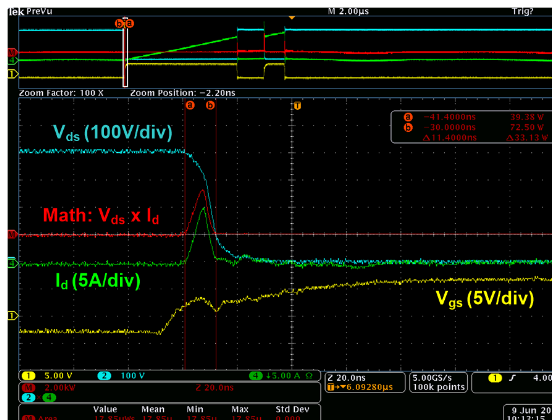

(d)

Fig. 15. E_{qoss} testing waveforms at (a) 100 V_{dc} with T_j=75°C and R_{g_on}=30 ohm, (b) 200 V_{dc} with T_j=25°C and R_{g_on}=30 ohm, (c) 300 V_{dc} with T_j=25°C and R_{g_on}=50 ohm, (d) 400 V_{dc} with T_j=75°C and R_{g_on}=30 ohm.

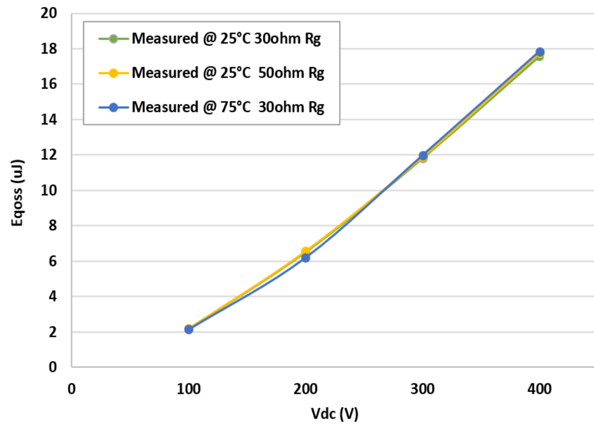

Fig. 16. Measured results with different T_j and R_g.

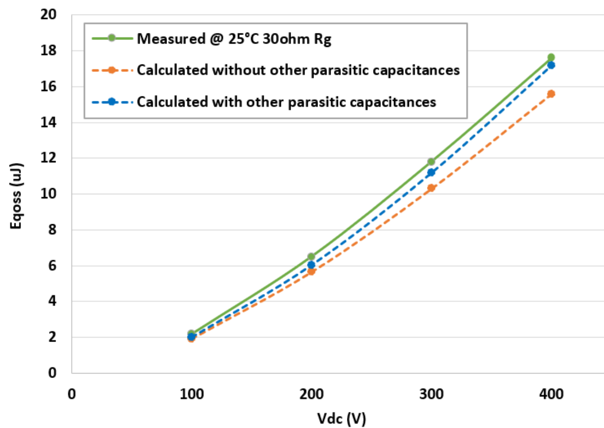

Fig. 17. Comparison between measurement and calculation results.

V. CONLUSIONS

In this paper, the detailed E_{qoss} loss mechanism, calculation and measurement method for GaN HEMTs are presented. The E_{qoss} loss of the active switch is contributed by the charging current mainly from the parasitic capacitance C_{oss} of the opposite switch in the half bridge. In addition, the loss is independent of load current, junction temperature and switching speed for general power electronic applications. A DPT platform with closed-loop temperature control is applied to validate the theory. Experimental results verify the E_{qoss} loss calculation method and also prove that the loss is only a function of voltage and the corresponding capacitances.

This E_{qoss} loss calculation can help engineers and researchers to calculate the switching-on energy loss of GaN and evaluate the overall efficiency of GaN-based systems more accurately.

REFERENCES

[1] E. A. Jones, F. Wang, and D. Costinett, "Review of commercial GaN power devices and GaN-based converter design challenges," *IEEE Journal of Emerging and Selected Topics in Power Electronics*, vol. 4, no. 3, pp. 707-719, Sept. 2016.

[2] J. Lu and D. Chen, "Paralleling GaN E-HEMTs in 10kW-100kW systems," in *Proc. 2017 IEEE Applied Power Electronics Conference and Exposition*, Tampa, FL, Mar. 2017, pp. 3049-3056.

[3] R. Xie, H. Wang, G. Tang, X. Yang, K. J. Chen, "An analytical model for false turn-on evaluation of high-voltage enhancement-mode GaN transistor in bridge-leg configuration," *IEEE Transactions on Power Electronics*, vol. 32, no. 8, pp. 6416-6433, Aug. 2017.

[4] H. Li, X. Zhang, Z. Zhang, C. Yao, F. Qi, B. Hu, J. Wang, and L. Liu, "Design of a 10 kW GaN-based high power density three-phase inverter," in *Proc. 2016 IEEE Energy Conversion Congress and Exposition*, Milwaukee, WI, Sept. 2016, pp. 1-8.

[5] W. Zhang, F. Wang, D. J. Costinett, L. M. Tolbert, and B. J. Blalock, "Investigation of gallium nitride devices in high-frequency LLC resonant converters," *IEEE Transactions on Power Electronics*. vol. 32, no. 1, pp. 571-583, Jan. 2017.

[6] R. Hou and A. Emadi, "Applied integrated active filter auxiliary power module for electrified vehicles with single-phase onboard chargers," *IEEE Transactions on Power Electronics*, vol. 32, no. 3, pp. 1860-1871, Mar. 2017.

[7] J. Lu, G. Liu, H. Bai, A. Brown, P. M. Johnson, M. McAmmond, and A. R. Taylor, "Applying variable-switching-frequency variable-phase-shift control and E-mode GaN HEMTs to an indirect matrix converter-based EV battery charger," *IEEE Transactions on Transportation Electrification*, vol. 3, no. 3, pp. 554-464, Sept. 2017.

[8] R. Hou and A. Emadi, "A primary full-integrated active filter auxiliary power module in electrified vehicles with single-phase onboard chargers," *IEEE Transactions on Power Electronics*. vol. 32, no. 11, pp. 8393-8405, Nov. 2017.

[9] J. Lu, A. R. Taylor, K. Bai, G. Liu, A. Brown, M. Johnson, and M. McAmmond, "A modular designed three-phase high-efficiency high-power-density EV battery charger using dual/triple-phase-shift control," *IEEE Transactions on Power Electronics*. Early access.

[10] F. Xue, R. Yu, and A. Q. Huang, "A 98.3% efficient GaN isolated bidirectional DC-DC converter for DC microgrid energy storage system applications," *IEEE Transactions on Industrial Electronics*, vol. 64, no. 11, pp. 9094-9103, Nov. 2017.

[11] Y. Qiu, L. Wang, H. Wang, Y. F. Liu, and P. C. Sen, "Bipolar ripple cancellation method to achieve single-stage electrolytic-capacitor-less high-power LED driver," *IEEE Journal of Emerging and Selected Topics in Power Electronics*, vol. 3, pp. 698-713, 2015.

[12] S. R. Bahl, D. Ruiz, and D. S. Lee, "Product-level reliability of GaN devices," in *Proc. 2016 IEEE International Reliability Physics Symposium*, Pasadena, CA, Apr. 2016.

[13] K. Wang, M. Tian, H. Li, F. Zhang, X. Yang, and L. Wang, "An improved switching loss model for a 650V enhancement-mode GaN transistor", in *Proc. 2016 IEEE Annual Southern Power Electronics Conference*, Auckland, New Zealand, Dec. 2016, pp. 1-6.

[14] E. A. Jones, F. Wang, D. Costinett, Z. Zhang, and B. Guo, "Temperature-dependent turn-on loss analysis for GaN HFETs," in *Proc. 2016 IEEE Applied Power Electronics Conference and Exposition*, Long beach, CA, Mar. 2016, pp. 1010-1017.

[15] R. Hou, J. Xu, and D. Chen, "Multivariable turn-on/turn-off switching loss scaling approach for high-voltage GaN HEMTs in a hard-switching half-bridge configuration," in *Proc. 2017 IEEE Wide Bandgap Power Devices and Applications*, Albuquerque, NM, Oct. 2017.

[16] GaN Systems Inc., GS66508T/GS66516T-EVBDB GaN E-HEMT Daughter Board and GS665MB-EVB Evaluation Platform, 2016. [Online]. Available: http://www.gansystems.com/gs66508t-evbdb.php.

[17] A. Huang, Infineon Technologies, Hard commutation of power MOSFET, 2014. [Online]. Available: https://www.infineon.com.

[18] P. Haaf and J. Harper, Fairchild Semiconductor, Understanding diode reverse recovery and its effect on switching losses, 2007. [Online]. https://www.fairchildsemi.com.